Enhancing photocatalytic performance of TiO_2 in H_2 evolution *via* Ru co-catalyst deposition

Weiyi Ouyang,[a] Mario J. Muñoz-Batista,[a] Anna Kubacka,[b] Rafael Luque,[a,c] and Marcos Fernández-García [*b]*

[a]*Departamento de Química Orgánica, Universidad de Córdoba, Edif. Marie Curie, Ctra Nnal IV-A, Km 396, E14014, Córdoba (Spain)*

[b]*Instituto de Catálisis y Petroleoquímica CSIC, Marie Curie 2, 28049 Madrid, Spain.*

[c]*Peoples Friendship University of Russia (RUDN University), 6 Miklukho-Maklaya Str., Moscow 117198, Russia*

Email: M.J. M-B (jmunoz385x@gmail.com), M. F-G (mfg@icp.csic.es)

Abstract

A series of ruthenium catalysts supported into pure anatase oxide were tested in the photo-production of hydrogen from methanol:water mixtures under UV and visible illumination conditions. Catalysts containing 1, 2, 3 and 5 wt.% of ruthenium were subjected to a characterization study with the help of X-ray diffraction, Raman, X-ray photoelectron spectroscopy, photoluminescence, morphology as well as scanning and transmission electron microscopy. Through the measurement of the optical properties of the suspension of the catalysts and the hydrogen photo-production reaction rate we calculate the true quantum efficiency. Optimum activity is presented by the catalyst with a 3 wt.% of Ru component, which shows quantum efficiency values of ca. 3.0 and 0.6 % under, respectively, UV and visible light illumination. Careful examination of the physico-chemical properties of the solid allows to establish a correlation between the ruthenium surface exposed and the quantum efficiency. The implications of such result to justify chemical activity of the ruthenium supported samples are discussed both for UV and visible illumination conditions.

Keywords

Photo-catalysis; titania; ruthenium, quantum efficiency, H_2 photo-production

Introduction

Photocatalytic materials play a role in the development of the new, greener society required for the XXI century by opening solutions for the protection of the environment as well as for the production of chemical energy vectors from sustainable materials and sources.[1–11] In this regards, hydrogen has received considerable attention as a next-generation energy carrier. One of the most interesting processes is the photo-water-splitting which is as a clean and renewable way to produce hydrogen using solar energy.[5,12–15] It has, however, some limitation. The overall water splitting reaction is an uphill reaction with a large positive change in Gibbs free energy. Besides, there is an activation barrier in the charge-transfer process between photocatalysts and water molecules, consequently a photon energy greater than the band gap of the photocatalyst to obtain reasonable reaction rates is necessary.[15] In this regard, a versatile reaction within the field of sustainable energy considers the production of hydrogen from raw materials extracted from bio-based processes and sunlight. Among them, the use of bioalcohols is common from the beginning of the research considering hydrogen photo-production. Methanol is the simple molecule among bio-alcohol and has been used as a model reactant in this photo-catalytic process.[16–21] The reaction is initiated by a hole attack to the alcohol and its further evolution in carbon-containing products, evolving protons concomitantly. The role of water in the reaction is complex but at least takes part in the activation of some specific carbon containing molecules such as aldehydes to produce carboxylates as well as to promote the evolution of this last species.[4,22] In any case, a critical point of the catalytic cycle is the electron attack to the protons to generate hydrogen. As well known, these reaction steps occur with the help of a co-catalyst to boost the reaction rates. Pt has been customarily utilized as it provides the higher reaction rates.[16,23,24]

Alternatives to Pt have been continuously essayed in the literature. In this search, other metal nobles such as Pd or Au showed similar activity.[19,25,26] However, for economic reasons, desirable alternatives would be out of these three noble metals. The use of non-noble metals has captured the attention of researchers with a significant number of works considering the use of Cu or Ni.[27–32] In relative contrast, the use of Ru has been significantly less explored. In fact, for the photo-production of hydrogen from bioalcohols, the use of ruthenium out of molecular complexes/compounds has been presented only in a single reference study to our knowledge.[33] The Ru-TiO_2 system showed relatively high activity but the study does not present an analysis of

the quantum efficiency of the reaction, limiting a possible quantitative comparison with results from other metals. In addition, Ru can provide interesting activity (compared with the most used noble metals as Pt, Pd and Au) under visible light illumination due to the inherent high absorption of the corresponding catalyst. Such capability relies on the existence of plasmon resonances directly ascribable to the Ru(IV) oxide.[34–36]

Here we will provide a study of the activity of Ru containing titania materials in the photo-production of hydrogen using a series of materials with growing quantities of ruthenium. As said, we particularly focus on measuring the activity on true basis by calculating the true quantum efficiency. This would allow quantitative comparison with other systems and thus to analyze the goodness of ruthenium for hydrogen photo-generation. According to the IUPAC recommendations, the calculation of the quantum efficiency requires the measurement of the reaction rate as well as the local volumetric rate of photon absorption.[37] To do it, we carried out the measurements of the optical properties of the catalysts suspensions and the modelling of the light-matter interaction at the reactor used to measure the catalytic properties. The study further considered with a complete characterization of the materials using X-ray diffraction (XRD), Raman, X-ray photoelectron spectroscopy (XPS), photoluminescence, porosimetry measurements, UV-visible spectroscopy as well as microscopy tools such as transmission and scanning microsocopies combined with electron dispersion x-ray analysis (EDX). With these tools, we attempt to rationalize the activity of the materials and particularly the maximization of the quantum efficiency occurring through the series of catalysts varying the ruthenium content. We also compared the performance of Ruthenium with Platinum/Palladium containing materials supported on pure anatase (or materials having a dominant anatase phase) from literature.

1. Experimental

1.1. Catalysts synthesis

1.1.1. Synthesis of TiO_2

In the present work, reversed micro-emulsion method was applied in the synthesis of TiO_2. Briefly, 177.4 mL Triton and 185.4 mL of hexanol were sequentially added into 854 mL n-heptane as surfactant and co-surfactant and mixed under stirring at 400 rpm for 30 minutes. Afterward, 100 MiliQ water was added to the above solution and the mixture was kept stirring

for 1 hour, followed by dropwise addition of titanium precursor solution (14.7 mL titanium isopropoxide dissolved into 24.4 mL isopropanol). The corresponding mixture was stirred overnight, then dispersion phase was removed using centrifugation for 15 minutes at 10000 rpm, 5 ^{o}C. The obtained solids were then washed with methanol under stirring (15 minutes) and recovered using centrifugation under the same conditions. The solids were dried at 70 ^{o}C for overnight after washing and then annealed at 600 ^{o}C for 30 minutes (ramping rate: 1 ^{o}C/min).

1.1.2. Incorporation of Ru on TiO_2

Firstly, 0.5 g TiO_2 was added to 100 mL MiliQ water, followed by sonication for 30 minutes. Then, a different amount of $RuCl_3 \cdot H_2O$ was added to the mixture to obtain 1, 2, 3, 5 wt. % loading of Ru on the TiO_2 support and sonicated for 5 minutes. Subsequently, an appropriate volume of 0.1 mol/L $NaBH_4$ solution (molar ratio, Ru: $NaBH_4$ = 1:5) was added to the mixture which was kept stirring for 1 hour. The above process was performed under N_2 bubbling protection. At last, the solids were recovered by centrifugation (10000 rpm, 15 min, 5 ^{o}C) and washed with deionized water, dried at 80 ^{o}C for overnight. The as-synthesized samples were named as 1 Ru/TiO_2, 2Ru/TiO_2, 3Ru/TiO_2 and 5Ru/TiO_2 respectively.

1.2.Characterization

Seifert D-500 diffractometer equipped with Ni-filtered Cu Kα radiation was employed to record XRD pattern of the as-synthesized samples with a 0.02° step. Raman spectra of samples were collected with an iHR320 Horiba Jobin-Yvon spectrometer equipped with a He:Ne laser (633 nm). Nitrogen physisorption was performed in Micromeritics ASAP 2010 for BET surface and porosimetry analysis. Scanning electron microscopy images were obtained using a JEOL JSM-7800 scanning microscope (SCAI of Universidad de Cordoba) equipped with EDX at 20 kV. Transmission electron microscopy images were taken in a JEOL 2100F TEM/STEM microscope. Elemental analysis was determined using inductively coupled plasma atomic absorption spectroscopy (ICP-OES) (PerkinElmer Optima 3300 DV). UV−vis transmission or diffuse-reflectance spectra were recorded with a Shimadzu UV2100 apparatus (using $BaSO_4$ as a reference for diffuse experiments). Photoluminescence spectra were measured at room temperature on a Fluorescence Spectrophotometer (Perkin Elmer LS50B). Trans- A VG Scientific photoelectron spectrometer ESCALAB-210 equipped with Mg Kα radiation (1486.6 eV) was used for the X-ray photoelectron spectroscopy (XPS) measurements, operated at 15 kV

and 20 mA. Survey spectra in the energy range from 0 to 1350 eV were recorded using 0.4 eV steps while high-resolution spectra were recorded with 0.1 eV steps, 100 ms dwell time and 25 eV pass energy. Curve fitting was carried out using the CasaXPS software in which aromatic carbon C1s peak (284.6 eV) was used as the reference for binding energy calibration.

1.3.Photocatalytic experiment

Photocatalytic H_2 production was performed in added 50 mL MeOH/H_2O solution (vol. ratio = 3:7) inside a double wall Pyrex reactor with a cooling system to control the temperature (25 ^{o}C), avoiding significant evaporation of the sacrificial agent. A 500 W Xe lamp was used as irradiation source, which was equipped with a light cut-off filter to select the desired wavelength (UV light: 280-400 nm; Visible light: 420-680 nm). 25 mg catalysts were suspended in the reaction solution with continuous stirring. The suspension was degassed with Ar stream (100 mL/min) for 30 min and then the Ar flow rate was set at 10 mL/min for the reaction. After 30 min at dark condition, the lamp was switched on with desired irradiation wavelength and the outlet gas was analyzed by an online mass spectroscopy.

1.4.Quantum efficiency calculation

Quantum Efficiency (Q.E.) parameter was used to compare and present the catalytic results. Q.E. is defined by Equation 1.[37]

$$Q.E.(\%) = 100 \times \frac{n \times r\ (\text{mol m}^{-3}\text{s}^{-1})}{e^{a}\ (\text{Einstein m}^{-3}\text{s}^{-1})} \qquad (1)$$

In this equation, r is the reaction rate and e^{a} the average local volumetric rate of photon absorption. n can be 1 or 2 depending of the reaction mechanism proposed in the literature (see details in the discussion section 6 “Mechanism” of the Supporting Information). e^{a} calculation requires the solution of the Radiative Transfer Equation (RTE) in the reactor which can be expressed by Equation 2.

Equation 2 describes the specific intensities, along the directional spatial coordinate (s). [23,38]

$$\frac{dI_{\lambda,\underline{\Omega}}(\underline{x})}{ds} = -\kappa_{\lambda} I_{\lambda,\underline{\Omega}}(\underline{x}) - \sigma_{\lambda} I_{\lambda,\underline{\Omega}}(\underline{x}) + \frac{\sigma_{\lambda}}{4\pi} \int_{\Omega'=4\pi} p(\underline{\Omega}' \rightarrow \underline{\Omega})\, I_{\lambda,\underline{\Omega}'} \qquad (2)$$

The solution of the integro-differential equation 2 provides the value of the intensity of photons for each differential elementary volume of the reactor and direction considered of radiation propagation and the wavelength. Its solution requires the determination of the optical parameters

(spectral absorption coefficient (κ_λ), spectral scattering coefficient (σ_λ) and scattering phase ($p\left(\underline{\Omega}' \rightarrow \underline{\Omega}\right)$). of the catalysts suspensions (See Supporting Information, section 3.1. Optical properties of the suspension. Solution of RTE for the spectrophotometer cell; one dimensional-one directional model). The scattering phase function was calculated using the Henyey and Greenstein which has been used with good results in similar optical systems.[38–40]

$$p\left(\underline{\Omega}' \rightarrow \underline{\Omega}\right) = \frac{1-g_\lambda^2}{\left(1+g_\lambda^2-2g_\lambda u_0\right)^{3/2}} \quad (3)$$

Where g_λ^2 is the asymmetry factor and u_0, the director cosine between ingoing at outgoing radiation. Extinction coefficients (β_λ were obtained by applying a standard linear regression to the plots of β_λ versus catalyst concentration C in a broad range (0.1-5 x 10^{-3} g L^{-1}). Optical properties were estimated by solving the RTE using the discrete ordinate method (MOD) in a rectangular spectrophotometer cell following a procedure developed previously.[39,41]

Once the optical properties of the catalyst(s) have been determined, the evaluation of the radiation field inside the photoreactor can be carried out. The MOD tool was used to transform the integro-differential Equation 2 into a system of algebraic equations that can be solved numerically. Complete procedure is detailed in the Supporting Information (Section 3.2. Optical properties of the suspension. Solution of RTE for the photoreactor setup; two dimensional-two directional model) and allows obtaining of e^a (local volumetric rate of photon absorption) at each point of the photoreactor.

$$e^a = \int_\lambda \kappa_\lambda \cdot \int_{\Omega=4\pi} I_{\lambda,\underline{\Omega}}\left(\underline{x}\right) d\Omega \, d\lambda \quad (6)$$

3. Results and discussion

3.1. Characterization

3.1.1. Structural and morphological analysis

The XRD diffraction patterns of the active TiO_2 support and Ru/TiO_2 photo-catalytic systems are displayed in Figure 1A. The analysis of the diffraction patterns only allowed the identification of Anatase phase; JCPDS card 78-2486, corresponding to the I41/amd space group. Raman analysis of titania also confirmed the absence of the Rutile phase in the titania support. As can be seen in Figure 1B and S3 of Supporting Information, the analysis only detected the presence of contributions at ca. 144, 195, 399, 517 and 639 cm^{-1} which can be exclusively ascribable to

Anatase phase.[42,43] For the composite materials, we highlight the lack of Rutile-type RuO_2 contributions, typically detected at 232, 447 and 612 cm^{-1} (results not shown).[44] This is confirmed by numerical calculation of crystallite size, microtensions and cell parameters of the anatase structure as it is summarized in Table 1. Crystallite size of the TiO_2 particles remain constant (c.a 16 +/- 2 nm) since the subsequent modification of the samples only targets a superficial stable deposition of Ru. Microtension and cell parameters also showed an unwavering character. In particular, doping of anatase can be disregarded. Morphological properties obtained by nitrogen physisorption are dominated by the major TiO_2 component. No noticeable effect can be detected in the morphological properties of the samples when the Ru component is deposited on the anatase structure (Table 1). Samples presented very similar BET surface area and porosity parameters which, as mentioned, is a consequence of the limited influence of the ruthenium compound deposition on the titania support structure.

The interaction between the components and the physico-chemical properties of the minor Ru component can be analyzed using XPS. Chemical composition of the surface was evaluated from the analysis of the C1s, Ti2p and Ru3p and Ru3d XPS regions. Analysis of Ru/TiO_2 samples corresponds to a relatively complex task taking into account that overlapping effects coming from close enough peak position(s) can be encountered between C-Ru and Ru-Ti contributions. [33,45] XPS information concerning Ti2p and Ru3p for the samples and the TiO_2 reference is graphically depicted in Figure 2A. Besides it, Figure 2B includes a representative example of the fitting procedure. Spectra presented in Figure 2A show that the binding energy of Ti2p peaks are located at 458.1 and 458.8 eV, values typical of the Ti(IV) oxidation state.[46] XPS $Ti2p_{3/2}$-$Ru3p_{5/2}$ energy region shows a relative low, but clearly defined increase of width (Table 3) which can be associated with the surface deposition of Ru. As can be seen in Figures 2A and 2B (fitting procedure; example for $2Ru/TiO_2$ sample) this energy region shows contributions which can be fitted considered a dominant Ru (IV) oxidation state. In particular, lines at 461.8 ($3p_{3/2}$) and 484.6 eV ($3p_{1/2}$) are typical of the Ru(IV) oxidation. [47,48] The same conclusion can be extracted from the Ru 3d XPS region (Figures 2C and 2D). Deconvolution analysis of all samples presented a well-defined contribution at c.a. 280.6 eV ($3d_{5/2}$) which are typical of the Ru (IV) oxidation state.[47–49] Taking into account the contribution of the $3d_{5/2}$ line, the final fitting approach shown in panel D of Figure 2 considers Ru3d (two) contributions and two more associated to different superficial carbonaceous species from spurious entities.[46] A summary

of XPS fitting results is presented in Table 2. XPS analysis, besides providing electronic information of the components, also allows carrying out an important elemental analysis of the surface. Although the chemical structure seems to be defined by the synthesis method, the exposed Ru concentration showed only a rough linear behaviour (Table 2). Figure 3 shows Ru/Ti atomic superficial concentration (Ru/Ti $_{XPS}$) as a function of Ru/Ti ratio obtained by ICP-OES (Ru/Ti $_{e.a}$). This ratio provides a more simple view or comparison of these observables. In both cases, the Ru/Ti ratio obviously increased as a consequence of the increasing of the Ru amount in the materials, although in the case of surface concentration, the 3Ru/TiO_2 seems above the linear trend suggested by the other three samples. This would indicate a relatively larger dispersion of the metal for this sample with respect to the remaining ones.

Aditional information about the nanostructured Ru/TiO_2 samples were obtained by SEM-mapping and TEM. Figures 4A and 4B show SEM micro-images of the two samples with Ru highest concentrations. It also included on both figures, the elemental mapping analysis. Mapping panels clearly show that Ti, O, C, and Ru elements are truly present in the samples. RuO_2 seems dispersed onto the support with reasonable homogeneity. In any case, no definitive conclusion regarded the Ru component distribution can be reached from these figures. Figure 5A-G presents representative TEM images for samples with 2, 3 and 5 wt. % of Ru. Detailed views of the materials show titania-platelet particles which have some smaller Ru particles on the surface. A proper particle size distribution can be obtained from the TEM analysis. Samples with 2, 3 and 5 wt. % were analyzed displaying the RuO_x size distribution presented in Figures 5H, 5I and 5J, respectively. The mean particle size for 2Ru/TiO_2 and 3Ru/TiO_2 obtained after counting more than 150 nanoparticles were c.a. 5 nm while the 5Ru/TiO2 showed an average size increase of about 2 nm was detected.

3.1.2. Optical properties analysis

For photocatalytic applications, optical properties and particularly the calculation of the light-matter interaction at the reactor are particularly relevant observables. In this work, we combine a typical UV-vis analysis with a strict calculation of Local Volumetric Rate of Photon Absorption (e^a). Starting with the UV-vis, samples presented UV-vis spectra dominated by the major TiO_2 component (Figure 6), displaying the characteristic intensity decay for a band gap energy of ca. 3.2 eV.[50] A gradual reduction of this parameter from 3.1 to 2.8 eV was detected with further

increasing of the Ru nanoparticles on the structure (Table 1). This combines with a significant absorption in the visible region derived from plasmon resonances of the ruthenium oxide. [34–36] This remarkable enhancement (with respect to the titania reference) of light appears, as mentioned, in the whole visible range, being potentially positive for the catalytic properties as will be discussed in next sections.

The band gap parameter describes the optical absorption but the calculation of Local Volumetric Rate of Photon Absorption gives the optical properties of the active material under the illumination condition used to obtain catalytic properties.[37] To do it, first, we must determine the optical properties of the catalytic suspension (Figure 7) using a spectrophotometric cell (See details of the modelling procedure in Supporting information). These optical properties allow the evaluation of the radiation field inside the photo-reactor from which the absorption profile through the reactor can be obtained (See details of the modelling procedure in Supporting information). Panels for the Local Volumetric Rate of Photon Absorption observable were expressed in two spatial coordinates according to the cylindrical geometry of the liquid reactor. They are presented in Figure 8. No appreciable differences, taking into account the model error, were observed among the catalysts studied under UV illumination condition (upper panels). However, as aforementioned, the enhancement of the absorption capability under visible conditions affects the Local Volumetric Rate of Photon Absorption observable. As can be seen in the lower row panels of Figure 8, an enhancement of this observable was detected under visible irradiation conditions. The most pronounced difference in comparison to TiO_2 references was obtained, as expected, for the 5Ru/TiO_2 sample (enhancement factor of 1.1).

3.2. Activity

During the photocatalytic methanol reforming process, several elemental steps can be considered. The mechanism has been studied using different technics and approaches (DRIFTs, GS-MS, Isotopic exchange experiments (D_2O), EPR, spectro-kinetic modeling, among others),[16–18,51–54] and can be summarized in the elemental steps presented in Table S2 of the Supporting Information. Steps (1-3) are based on the well-established initial elemental steps of photocatalytic processes: (1) the photo-excited sample generates electrons and holes, (2) holes may react with adsorbed water and superficial OH·ions to generate hydroxyl radicals, and (3) recombination of electrons and holes and the resulting loss of energy.[55,56] According to the

reaction scheme of previous reports, the oxidations steps can occur through a direct or indirect path using (h^+) or ($OH^\bullet$) radical species, respectively (Table S2).[16] Is important to mention that, a process called "current-doubling effect" can happen. In this case, the hole-capture species is transformed to a radical anion intermediate and then injects an electron into the conduction band of the catalyst.[52–54] This process, associated with equations (5-6), would imply that only one photon would be necessary to produce one hydrogen molecule. Alternatively (equation 7) a second hydroxyl radical can interact with the organic radical anion and would render a product of the reaction.

As it is described in the previous section, catalytic properties of the samples were evaluated by using both the reaction rate and the quantum efficiency observables. Quantum efficiency is not only the IUPAC recommended way to present photocatalytic results but also a general parameter to carry out quantitative comparisons with other literature data.[37,57] As aforementioned, the value of n in Equation 1 (and Equation S5-S6) will depends of the number of electron and proton available to produce H_2. In others word, n value will be 1 if "current-doubling effect" is taking into account. In contrast, if it is assumed that the transfer of two electrons is required to reduce tow protons and thus to produce one H_2 molecule, n is equal to 2. Table XS of Supporting Information presents Q.E. values considering both assumptions. The photonic efficiency (P.E.), also called Apparent Quantum Efficiency,[58] have been also calculated and presented in Table S1 of supporting information. Q.E. shows higher values for both irradiation sources, in comparison with the values obtained for the P.E. The most active sample ($3Ru/TiO_2$) shows enhancement factors (Q.E. vs. P.E.) of 1.1 and 1.2 for UV and ST illumination conditions, respectively.

Figure 9 summarizes reaction rate (mol m^{-3} s^{-1}) and quantum efficiency (Einstein m^{-3} s^{-1}) values obtained under both UV and visible irradiation. Q.E. represented in Figure 9 were obtained assuming 2 for the n value. This allows comparison with literature in which 2 photons were counted during the Q.E. calculation. Reaction rate shows that all samples containing the Ru co-catalyst display enhanced activity with respect to the support, with a clear maximum situated at about 2-3 wt. % of Ru. Focusing on quantum efficiency; values of 3.0 and 0.6 % were obtained for UV and visible illumination conditions, respectively. Comparison with literature reports is relatively difficult. Ru supported on titania materials have been tested recently for CO_2 photo-reduction showing the importance of the Ru metallic state to boost activity.[59] More classical

studies of Ru promoted titania materials concern the photo-degradation of dyes.[60] To our knowledge, a single reference concerns the publication of previous results for methanol photo-reforming using Ru on titania materials. A sample having a 0.7 wt. % of Ru rendered an apparent quantum efficiency of 1.2 % under UV light. [33] This can be compared with a value of 2.8 calculated for the $3Ru/TiO_2$ sample. We thus multiply by ca. 2.4 the previous result of a ruthenium-based catalyst. Note that our material having similar Ru content (the $1Ru/TiO_2$ sample) also displays a larger apparent quantum efficiency value, 1.8 %. Finally, it is interesting to note that the quantum efficiency allows calculating the expected activity of the materials for solar light application. The $3Ru/TiO_2$ sample would render c.a. 1.1 quantum efficiency value under sunlight (AM1.5 standard).

In order to explore the influence of charge mobility/recombination process, we have measured photoluminescence of Ru/TiO_2 samples (Figure 10A and B) under UV (320 nm) and visible (450 nm) excitation, respectively. Spectra are dominated by two kinds of transitions corresponding to the annihilation of conduction band free electrons with trapped holes and valence band free holes with trapped electrons.[19,61] The profiles obtained show very similar behaviour and broad peaks at ca. 425, 480 and 500 (UV excitation) and 615 and 640 (visible excitation) nm, dominated by the anatase major component, which is in accordance with previous reports of co-catalysts-titania materials. [19,23,58,61] As aforementioned, samples display very marginal differences which allow the adequate yet simple analysis of recombination in terms of the overall intensity. Thus we can note that the most active sample ($3Ru/TiO_2$) present lower photoluminescence intensity under both UV and VIS irradiation conditions. This would indicate that the interaction between the Ru compound-titania favours the decrease of the charge recombination with respect to the titania reference, irrespective of the light wavelength.

As summarized in Table 4, comparison with Pt or Pd samples over titania support is rather interesting. $1Ru/TiO_2$ and $3Ru/TiO_2$ samples render comparable results compared with samples in which Pt and Pd were deposited on a Nb-doped titania previously synthesized by a microwave-assisted method.[19] The optimum quantum efficiency value obtained for Ru-containing ($3Ru/TiO_2$) and Pt-containing (1 wt. % of platinum onto a Nd-doped titania obtained by reverse microemulsion method) samples using the same reaction setup indicates larger values (ca. 40 %) with respect to Pd but lower values (40 %) with respect to Pt.[23] Activity of ruthenium samples is thus competitive, even when compared with Pt, considering that the price

of a ruthenium-based catalyst would significantly reduce with respect to platinum-palladium-based ones.

Within our series of samples, it seems clear that the increase of Ru concentration increases the size of the ruthenium oxide nanoparticles (Figure 3), which in turn translates into a more heterogeneous distribution (Figure 5G-I). Additionally, the variation of the behaviour of the surface concentration vs the bulk counterpart seems to have a significant influence on the activity. In fact, as it is shown in Figure 11, the relationship between the surface (measured with XPS) and bulk (measured with ICP-OES) Ru/Ti ratios describes a similar profile than the quantum efficiency of the samples for both illumination sources tested in the work. This result suggests that ruthenium superficial concentration interface plays an important role on the activity of our samples. Such a conclusion would, in fact, indicate a cooperative catalytic effect grounded in several factors; size and distribution of RuO_2 nanoparticles, increasing visible light absorption with Ru content and a positive photo handling of charge carrier after excitation. The photo-handling of charge carriers through the interface would be dependent on the ruthenium loading. The band gap of nanometer RuO_2 type particles strongly depends on the primary particle size, defect structure and crystallinity, going from a value of ca. 2.1 typical of the bulk oxide to below of 1.5 eV.[62,63]. While the bulk oxide is likely a hole acceptor while in contact with anatase, the large shift of the conduction and valence bands observed for some nanosized materials does not allow to make a clear statement in the case of supported Ru-containing oxide clusters. Here they appear to power the electron collection to render hydrogen in a direct or, more likely, an indirect way by generating adequate interface sites with titania to handle electrons created though titania excitation and/or ruthenium oxide plasmon resonances. Surface sites at the ruthenium oxide - titania interface have been shown to play a role in promoting photo-oxidation with respect to the bare titania reference. [*J. Phys. Chem. C, 117, 11149-11158 (2013)]* The exact role of the interface in our case remains however to be verified but the nanometer size (with concomitant defect structure likely affected by both size and interface effects with titania) of the Ru-containing component at the titania-based materials does not allow an easy study of this point using the collection of spectroscopies here utilized. Only the use of nanometer size (excitation) beams for spectroscopic tools (for example in UPS/XPS) would allow the obtaining of further information. However, this technology is currently not available.

In spite that the unknown exact mechanism by which the Ru/TiO_2 showed high activity in hydrogen photo-production, all the above mentioned physical phenomena would contribute to the activity of the Ru titania composite samples. The maximum of activity in our case seems related to the control of the primary particle size of Ru component and the simultaneous maximization of the three factors just mentioned. This optimum combination is achieved with the $3Ru/TiO_2$ sample.

4. Conclusions

A series of ruthenium-based catalysts with weight loadings from 1 to 5 % were deposited using a chemical reduction method into a highly crystalline anatase support. The support appears essentially unaltered by the deposition method. The resulting noble metal phase appears an oxidized Ru(IV) type phase in all cases. This component has an average primary particle size below 5 nm for loadings equal to or below 3 wt % and around 7 nm for the $5Ru/TiO_2$ sample. Introduction of the Ru component alters significantly the optical properties, particularly in the visible region, of the catalysts with respect to the bare support. This can be ascribed to RuO_2 plasmon resonance related effects.

The photo-activity of the samples for methanol photo-reforming was investigated through the measurement of the hydrogen photo-production reaction rate and quantum efficiency values. The activity under both UV and visible illumination increases in presence Ru up to a loading of 3 wt. %. For the $3Ru/TiO_2$ catalyst we obtained quantum efficiency values of ca. 3.0 and 0.6 % for, respectively, UV and visible light illumination. The comparison of catalytic data with the ratio between surface and bulk values of the Ru/Ti observable indicates that ruthenium superficial concentration itself and/or the Ru oxide - titania interface play an important role(s) in driving the activity of our samples. As this result appears for all illumination conditions, we would suggest that charge recombination is a key property in driving the activity of the materials. However, in addition to this property, we highlight the importance of the visible light performance of the catalysts, mostly relying on the surface plasmon resonance of the ruthenium oxide.

Acknowledgments

A. Kubacka and M. Fernández-García is thankful to MINECO (Spain) for supporting the work carried out through the ENE2016-77798-C4-1-R grant. Mario J. Munoz-Batista gratefully acknowledges MINECO for a JdC contract (Ref. FJCI-2016-29014). Rafael Luque funding from the European Union's Horizon 2020 research and innovation programme under the Marie Sklodowska- Curie grant agreement No. 641861 (for funding Weyi Ouyang Ph.D studies). The publication has been prepared with support of RUDN University Program 5-100.

References

[1] D. Ravelli, D. Dondi, M. Fagnoni, A. Albini, Photocatalysis. A multi-faceted concept for green chemistry, Chem. Soc. Rev. 38 (2009) 1999–2011. doi:10.1039/b714786b.

[2] J.C. Colmenares, R. Luque, Heterogeneous photocatalytic nanomaterials: prospects and challenges in selective transformations of biomass-derived compounds, Chem. Soc. Rev. 43 (2014) 765–778. doi:10.1039/C3CS60262A.

[3] L. Yuan, N. Zhang, Y.-J. Xu, J.C. Colmenares, Solar–Chemical Energy Conversion by Photocatalysis, in: Heterog. Photocatal., Springer, Berlin, Heidelberg, 2016: pp. 249–282. doi:10.1007/978-3-662-48719-8_8.

[4] A. Kubacka, M. Fernández-García, G. Colón, Advanced nanoarchitectures for solar photocatalytic applications., Chem. Rev. 112 (2012) 1555–1614. doi:10.1021/cr100454n.

[5] M.-Q. Yang, N. Zhang, M. Pagliaro, Y.-J. Xu, Artificial photosynthesis over graphene–semiconductor composites. Are we getting better?, Chem. Soc. Rev. 43 (2014) 8240–8254. doi:10.1039/C4CS00213J.

[6] S. Liu, C. Han, Z.-R. Tang, Y.-J. Xu, Heterostructured semiconductor nanowire arrays for artificial photosynthesis, Mater. Horizons. 3 (2016) 270–282. doi:10.1039/C6MH00063K.

[7] L. Yuan, C. Han, M.-Q. Yang, Y.-J. Xu, Photocatalytic water splitting for solar hydrogen generation: fundamentals and recent advancements, Int. Rev. Phys. Chem. 35 (2016) 1–36. doi:10.1080/0144235X.2015.1127027.

[8] J. Ran, T.Y. Ma, G. Gao, X.-W. Du, S.Z. Qiao, Porous P-doped graphitic carbon nitride nanosheets for synergistically enhanced visible-light photocatalytic H2 production, Energy Environ. Sci. 8 (2015) 3708–3717. doi:10.1039/C5EE02650D.

[9] J. Ran, X. Wang, B. Zhu, S.-Z. Qiao, Strongly interactive 0D/2D hetero-structure of a ZnxCd1−xS nano-particle decorated phosphorene nano-sheet for enhanced visible-light photocatalytic H 2 production, Chem. Commun. 53 (2017) 9882–9885. doi:10.1039/C7CC05466A.

[10] B. Weng, S. Liu, Z.-R. Tang, Y.-J. Xu, One-dimensional nanostructure based materials for versatile photocatalytic applications, RSC Adv. 4 (2014) 12685–12700. doi:10.1039/c3ra47910b.

[11] J.C. Colmenares, R.F. Colmenares Quintero, I.S. Pieta, Catalytic Dry Reforming for Biomass-Based Fuels Processing: Progress and Future Perspectives, Energy Technol. 4 (2016) 881–890. doi:10.1002/ente.201600195.

[12] G. Editors, D. Nocera, D. Guldi, Renewable Energy issue energy research, Chem. Soc. Rev. 38 (2009) 253–278. doi:10.1039/b800489g.

[13] K. Maeda, K. Domen, Photocatalytic Water Splitting: Recent Progress and Future Challenges, J. Org. Chem. Lett. 1 (2010) 2655–2661. doi:10.1021/jz1007966.

[14] X. Li, J. Yu, Water Splitting By Photocatalytic Reduction, in: Water Split. By Photocatalytic Reduct., Springer, Berlin, Heidelberg, 2016: pp. 175–210. doi:10.1007/978-3-662-48719-8_6.

[15] K. Maeda, K. Domen, New non-oxide photocatalysts designed for overall water splitting under visible light, J. Phys. Chem. C. 111 (2007) 7851–7861. doi:10.1021/jp070911w.

[16] G.L. Chiarello, D. Ferri, E. Selli, Effect of the CH3OH/H2O ratio on the mechanism of the gas-phase photocatalytic reforming of methanol on noble metal-modified TiO2, J. Catal. 280 (2011) 168–177. doi:10.1016/j.jcat.2011.03.013.

[17] G.L. Chiarello, M.H. Aguirre, E. Selli, Hydrogen production by photocatalytic steam reforming of methanol on noble metal-modified TiO2, J. Catal. 273 (2010) 182–190. doi:10.1016/j.jcat.2010.05.012.

[18] O. Fontelles-Carceller, M.J. Muñoz-Batista, J.C. Conesa, A. Kubacka, M. Fernández-García, H2 photo-production from methanol, ethanol and 2-propanol: Pt-(Nb)TiO2 performance under UV and visible light, Mol. Catal. 446 (2018) 88–97. doi:10.1016/j.mcat.2017.12.023.

[19] U. Caudillo-Flores, M.J. Muñoz-Batista, J.A. Cortés, M. Fernández-García, A. Kubacka, UV and visible light driven H2 photo-production using Nb-doped TiO2: Comparing Pt and Pd co-catalysts, Mol. Catal. 437 (2017) 1–10. doi:10.1016/j.mcat.2017.04.035.

[20] G. Wu, T. Chen, W. Su, G. Zhou, X. Zong, Z. Lei, C. Li, H2 production with ultra-low CO selectivity via photocatalytic reforming of methanol on Au/TiO2 catalyst, Int. J. Hydrogen Energy. 33 (2008) 1243–1251. doi:10.1016/J.IJHYDENE.2007.12.020.

[21] A.A. Nada, H.A. Hamed, M.H. Barakat, N.R. Mohamed, T.N. Veziroglu, Enhancement of photocatalytic hydrogen production rate using photosensitized TiO2/RuO2-MV2+, Int. J. Hydrogen Energy. 33 (2008) 3264–3269. doi:10.1016/j.ijhydene.2008.04.027.

[22] M.R. Hoffmann, S.T. Martin, W. Choi, D.W. Bahnemannt, Environmental Applications of Semiconductor Photocatalysis, Chem. Rev. 95 (1995) 69–96. doi:10.1021/cr00033a004.

[23] O. Fontelles-Carceller, M.J. Muñoz-Batista, J.C. Conesa, M. Fernández-García, A. Kubacka, UV and visible hydrogen photo-production using Pt promoted Nb-doped TiO2 photo-catalysts: Interpreting quantum efficiency, Appl. Catal. B Environ. 216 (2017) 133–145. doi:10.1016/j.apcatb.2017.05.022.

[24] M.J. Muñoz-Batista, D. Rodríguez-Padrón, A.R. Puente-Santiago, A. Kubacka, R. Luque, M. Fernández-García, Sunlight-Driven Hydrogen Production Using an Annular Flow Photoreactor and g-C3N4-Based Catalysts, ChemPhotoChem. (2018) 1–9. doi:10.1002/cptc.201800064.

[25] R. Su, R. Tiruvalam, A.J. Logsdail, Q. He, C.A. Downing, M.T. Jensen, N. Dimitratos, L. Kesavan, P.P. Wells, R. Bechstein, H.H. Jensen, S. Wendt, C.R.A. Catlow, C.J. Kiely, G.J. Hutchings, F. Besenbacher, Designer Titania-Supported Au–Pd Nanoparticles for Efficient Photocatalytic Hydrogen Production, ACS Nano. 8 (2014) 3490–3497. doi:10.1021/nn500963m.

[26] T. Sreethawong, S. Yoshikawa, Comparative investigation on photocatalytic hydrogen evolution over Cu-, Pd-, and Au-loaded mesoporous TiO2 photocatalysts, Catal. Commun. 6 (2005) 661–668. doi:10.1016/j.catcom.2005.06.004.

[27] S. Obregón, M.J. Muñoz-Batista, M. Fernández-García, A. Kubacka, G. Colón, Cu–TiO2 systems for the photocatalytic H2 production: Influence of structural and surface support

features, Appl. Catal. B Environ. 179 (2015) 468–478. doi:10.1016/j.apcatb.2015.05.043.

[28] A. Kubacka, M.J. Muñoz-Batista, M. Fernández-García, S. Obregón, G. Colón, Evolution of H2 photoproduction with Cu content on CuOx-TiO2 composite catalysts prepared by a microemulsion method, Appl. Catal. B Environ. 163 (2015) 214–222. doi:10.1016/j.apcatb.2014.08.005.

[29] M.J. Muñoz-Batista, D. Motta Meira, G. Colón, A. Kubacka, M. Fernández-García, Phase-Contact Engineering in Mono- and Bimetallic Cu-Ni Co-catalysts for Hydrogen Photocatalytic Materials, Angew. Chemie - Int. Ed. 57 (2018) 1199–1203. doi:10.1002/anie.201709552.

[30] D. Barreca, P. Fornasiero, A. Gasparotto, V. Gombac, C. Maccato, T. Montini, E. Tondello, The Potential of Supported Cu2O and CuO Nanosystems in Photocatalytic H2 Production, ChemSusChem. 2 (2009) 230–233. doi:10.1002/cssc.200900032.

[31] S. Shen, L. Zhao, Z. Zhou, L. Guo, Enhanced Photocatalytic Hydrogen Evolution over Cu-Doped ZnIn2S4 under Visible Light Irradiation, J. Phys. Chem. C. 112 (2008) 16148–16155. doi:10.1021/jp804525q.

[32] T. Montini, V. Gombac, L. Sordelli, J.J. Delgado, X. Chen, G. Adami, P. Fornasiero, Nanostructured Cu/TiO2 Photocatalysts for H2 Production from Ethanol and Glycerol Aqueous Solutions., ChemCatChem. 3 (2011) 574–577. doi:10.1002/cctc.201000289.

[33] Q. Gu, J. Long, L. Fan, L. Chen, L. Zhao, H. Lin, X. Wang, Single-site Sn-grafted Ru/TiO2 photocatalysts for biomass reforming: Synergistic effect of dual co-catalysts and molecular mechanism, J. Catal. 303 (2013) 141–155. doi:10.1016/j.jcat.2013.03.014.

[34] A.D. Dunkelberger, R. Compton, P.A. Desario, D. Weidinger, B.T. Spann, I.R. Pala, C.N. Chervin, D.R. Rolison, K. Bussmann, P.D. Cunningham, J.S. Melinger, B.G. Alberding, E.J. Heilweil, J.C. Owrutsky, Transient Optical and Terahertz Spectroscopy of Nanoscale Films of RuO 2, (2017) 743–750. doi:10.1007/s11468-016-0321-3.

[35] M.A. Asi, C. He, M. Su, D. Xia, L. Lin, H. Deng, Y. Xiong, R. Qiu, X. Li, Photocatalytic reduction of CO 2 to hydrocarbons using AgBr/TiO 2 nanocomposites under visible light, Catal. Today. 175 (2011) 256–263. doi:10.1016/j.cej.2018.04.094.

[36] M.T. Uddin, Y. Nicolas, C. Olivier, L. Servant, T. Toupance, S. Li, A. Klein, W.

Jaegermann, Improved photocatalytic activity in RuO2–ZnO nanoparticulate heterostructures due to inhomogeneous space charge effects, Phys. Chem. Chem. Phys. 17 (2015) 5090–5102. doi:10.1039/C4CP04780J.

[37] S.E. Braslavsky, A.M. Braun, A.E. Cassano, A. V. Emeline, M.I. Litter, L. Palmisano, V.N. Parmon, N. Serpone, Glossary of terms used in photocatalysis and radiation catalysis (IUPAC Recommendations 2011), Pure Appl. Chem. 83 (2011) 931–1014. doi:10.1351/PAC-REC-09-09-36.

[38] J. Marugán, R. van Grieken, A.E. Cassano, O.M. Alfano, Intrinsic kinetic modeling with explicit radiation absorption effects of the photocatalytic oxidation of cyanide with TiO2 and silica-supported TiO2 suspensions, Appl. Catal. B Environ. 85 (2008) 48–60. doi:10.1016/j.apcatb.2008.06.026.

[39] María L. Satuf, Rodolfo J. Brandi, A.E. Cassano, O.M. Alfano, Experimental Method to Evaluate the Optical Properties of Aqueous Titanium Dioxide Suspensions, 44 (2005) 6643–6649. doi:10.1021/ie050365y.

[40] G. Camera-roda, V. Loddo, L. Palmisano, F. Parrino, Guidelines for the assessment of the rate law of slurry photocatalytic reactions, Catal. Today. 281 (2017) 221–230. doi:10.1016/j.cattod.2016.06.050.

[41] M.I. Cabrera, O.M. Alfano, A.E. Cassano, María I. Cabrera, Absorption and Scattering Coefficients of Titanium Dioxide Particulate Suspensions in Water, J. Phys. Chem. 100 (1996) 20043–20050. doi:10.1021/jp962095q.

[42] M. Mikami, S. Nakamura, O. Kitao, H. Arakawa, Lattice dynamics and dielectric properties of TiO2 anatase: A first-principles study, Phys. Rev. B. 66 (2002) 155213. doi:10.1103/PhysRevB.66.155213.

[43] * M. Fernández-García, A. Martínez-Arias, and A. Fuerte, J.C. Conesa, Nanostructured Ti−W Mixed-Metal Oxides: Structural and Electronic Properties, (2005). doi:10.1021/JP0465884.

[44] L.M. Martínez Tejada, A. Munõz, M.A. Centeno, J.A. Odriozola, In-situ Raman spectroscopy study of Ru/TiO2catalyst in the selective methanation of CO, J. Raman Spectrosc. 47 (2016) 189–197. doi:10.1002/jrs.4774.

[45] Q. Gu, Z. Gao, S. Yu, C. Xue, Constructing Ru/TiO2 Heteronanostructures Toward Enhanced Photocatalytic Water Splitting via a RuO2/TiO2 Heterojunction and Ru/TiO2 Schottky Junction, Adv. Mater. Interfaces. 3 (2016) 17–21. doi:10.1002/admi.201500631.

[46] M.J. Muñoz-Batista, A. Kubacka, M.N. Gómez-Cerezo, D. Tudela, M. Fernández-García, Sunlight-driven toluene photo-elimination using CeO2-TiO2 composite systems: A kinetic study, Appl. Catal. B Environ. 140–141 (2013) 626–635. doi:10.1016/j.apcatb.2013.04.071.

[47] Christina Bock, Chantal Paquet, Martin Couillard, Gianluigi A. Botton, B.R. MacDougall, Size-Selected Synthesis of PtRu Nano-Catalysts: Reaction and Size Control Mechanism, J. Am. Chem. Soc. (2004) 8028–8037. doi:10.1021/JA0495819.

[48] E.A. Paoli, F. Masini, R. Frydendal, D. Deiana, C. Schlaup, M. Malizia, T.W. Hansen, S. Horch, I.E.L. Stephens, I. Chorkendorff, Oxygen evolution on well-characterized mass-selected Ru and RuO2 nanoparticles, Chem. Sci. 6 (2015) 190–196. doi:10.1039/C4SC02685C.

[49] S. Kundu, A.B. Vidal, M.A. Nadeem, S.D. Senanayake, H. Idriss, P. Liu, J.A. Rodriguez, D. Stacchiola, Ethanol Photoreaction on RuOx/Ru-Modified TiO2 (110), J. Phys. Chem. C. 117 (2013) 11149–11158. doi:10.1021/jp4015367.

[50] M.J. Muñoz-Batista, A. Kubacka, M. Fernández-García, Effect of g-C3N4 loading on TiO2-based photocatalysts: UV and visible degradation of toluene, Catal. Sci. Technol. 4 (2014) 2006–2015. doi:10.1039/c4cy00226a.

[51] G.L. Chiarello, L. Forni, E. Selli, Photocatalytic hydrogen production by liquid- and gas-phase reforming of CH3OH over flame-made TiO2 and Au/TiO2, Catal. Today. 144 (2009) 69–74. doi:10.1016/j.cattod.2009.01.023.

[52] O.I. Micic, Y. Zhang, K.R. Cromack, A.D. Trifunac, M.C. Thurnauer, Trapped holes on titania colloids studied by electron paramagnetic resonance, J. Phys. Chem. 97 (1993) 7277–7283. doi:10.1021/j100130a026.

[53] A. Yamakata, T. Ishibashi, H. Onishi, Electron- and Hole-Capture Reactions on Pt/TiO2 Photocatalyst Exposed to Methanol Vapor Studied with Time-Resolved Infrared Absorption Spectroscopy, J. Phys. Chem. B. 106 (2002) 9122–9125.

doi:10.1021/jp025993x.

[54] J. Hansen, R. Bebensee, U. Martinez, S. Porsgaard, E. Lira, Y. Wei, L. Lammich, Z. Li, H. Idriss, F. Besenbacher, B. Hammer, S. Wendt, Unravelling Site-Specific Photo-Reactions of Ethanol on Rutile TiO2(110), Sci. Rep. 6 (2016) 1–11. doi:10.1038/srep21990.

[55] M.J. Muñoz-Batista, A.M. Eslava-Castillo, A. Kubacka, M. Fernández-García, Thermo-photo degradation of 2-propanol using a composite ceria-titania catalyst: Physico-chemical interpretation from a kinetic model, Appl. Catal. B Environ. 225 (2018) 298–306. doi:10.1016/j.apcatb.2017.11.073.

[56] M.J.J. Muñoz-Batista, M.M.M. Ballari, A.E.E. Cassano, O.M.M. Alfano, A. Kubacka, M. Fernández-García, Ceria promotion of acetaldehyde photo-oxidation in a TiO 2 -based catalyst: a spectroscopic and kinetic study, Catal. Sci. Technol. 5 (2014) 1521–1531. doi:10.1039/C4CY01293C.

[57] I.E. Wachs, S.P. Phivilay, C.A. Roberts, Reporting of Reactivity for Heterogeneous Photocatalysis, ACS Catal. 3 (2013) 2606–2611. doi:10.1021/cs4005979.

[58] O. Fontelles-Carceller, M.J. Muñoz-Batista, E. Rodríguez-Castellón, J.C. Conesa, M. Fernández-García, A. Kubacka, Measuring and interpreting quantum efficiency for hydrogen photo-production using Pt-titania catalysts, J. Catal. 347 (2017) 157–169. doi:10.1016/j.jcat.2017.01.012.

[59] L. Lin, K. Wang, K. Yang, X. Chen, X. Fu, W. Dai, The visible-light-assisted thermocatalytic methanation of CO2 over Ru/TiO(2-x)Nx, Appl. Catal. B Environ. 204 (2017) 440–455. doi:10.1016/J.APCATB.2016.11.054.

[60] A.O. Ibhadon, G.M. Greenway, Y. Yue, P. Falaras, D. Tsoukleris, The photocatalytic activity of TiO2 foam and surface modified binary oxide titania nanoparticles, J. Photochem. Photobiol. A Chem. 197 (2008) 321–328. doi:10.1016/J.JPHOTOCHEM.2008.01.010.

[61] T. Tachikawa, T. Majima, Exploring the Spatial Distribution and Transport Behavior of Charge Carriers in a Single Titania Nanowire, J. Am. Chem. Soc. 131 (2009) 8485–8495. doi:10.1021/ja900194m.

[62] M.A. Khan, D.H. Han, O.-B. Yang, Enhanced photoresponse towards visible light in Ru

doped titania nanotube, Appl. Surf. Sci. 255 (2009) 3687–3690. doi:10.1016/J.APSUSC.2008.10.021.

[63] F. El-Tantawy, A.A. Al-Ghamdi, A.A. Al-Ghamdi, Y.A. Al-Turki, A. Alshahrie, F. Al-Hazmi, O.A. Al-Hartomy, Optical properties of nanostructured ruthenium dioxide thin films via sol–gel approach, J. Mater. Sci. Mater. Electron. 28 (2017) 52–59. doi:10.1007/s10854-016-5491-4.

Table 1. XRD-derived size, microstrain and cell parameters for TiO_2 Anatase phase.

Sample	Size (nm) TiO_2	Microstrain $<\xi^2>^{1/2}$ (x 10^{-3}) TiO_2	TiO_2 Anatase Cell parameters (Å) a=b	c
TiO_2	16.4	1.80	3.786	9.497
1Ru/TiO_2	16.2	1.61	3.786	9.498
2Ru/TiO_2	16.5	1.58	3.783	9.493
3Ru/TiO_2	16.1	1.92	3.785	9.491
5Ru/TiO_2	16.5	1.59	3.783	9.491

Table 2. Band Gap and morphological properties of Ru/TiO_2 samples and TiO_2 reference.

sample	Band gap (eV)	BET surface area (m^2 g^{-1})	pore volume (cm^3 g^{-1})	pore size (nm)
TiO_2	3.1_5	44	0.097	8.33
1Ru/TiO_2	3.0	46	0.103	7.56
2Ru/TiO_2	3.0	47	0.104	7.37
3Ru/TiO_2	2.9	47	0.109	7.70
5Ru/TiO_2	2.8	47	0.111	7.76

Table 3. XPS Data for the xRu/TiO_2 samples

Sample	Ti2p3/2 (eV)	Ti2$p_{1/2}$-~~Ru3$p_{3/2}$~~ width (eV)[a]	Ru3d5/2 (eV)	O1s (eV)	Ru/Ti at. %	Ru/Ti at. (ICP-OES)
TiO_2	458.3	2.2[a]	-	529.8	-	-
1Ru/TiO_2	458.3	2.4	280.7	529.7	0.287	0.003
2Ru/TiO_2	458.4	2.4	280.8	529.8	0.409	0.006
3Ru/TiO_2	458.4	2.5	280.8	529.7	0.432	0.008
5Ru/TiO_2	458.4	2.5	280.6	529.7	0.697	0.011

[a] width only ascribable to the Ti2$p_{1/2}$ component

Table 4. Comparison of quantum efficiency values for the1Ru/TiO_2 and 3Ru/TiO_2 samples and Pt/Pd co-catalysts titania-based samples under UV and Sunlight-type (S.T.) illumination conditions.

Sample	Novel metal wt. %	UV Q.E (%)	S.T Q.E. (%)	Reference
1Ru/TiO_2	1	2.3	0.1	This work
3Ru/TiO_2	3	3.1	0.6	This work
0.025NbTi/Pt[a]	1	5.1	2.5	[23]
3NbTi/Pt[b]	1	1.9	1.6	[19]
3NbTi/Pd[c]	1	0.0_6	0.0_1	[19]

[a]0.025NbTi/Pt: 1 wt. % of Pt on Nb-doped Titania. (Titania doped with 2.5 Nb mol. %)
[b]3NbTi/Pt: 1 wt. % of Pt on Nb-doped Titania. (Titania doped with 3 Nb mol. %)
[c]3NbTi/Pd: 1 wt. % of Pd on Nb-doped Titania. (Titania doped with 3 Nb mol. %)

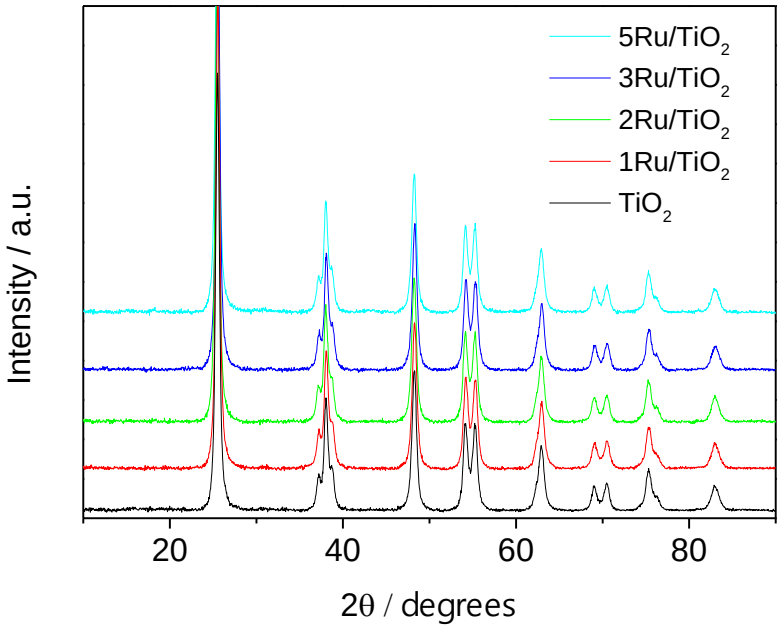

Figure 1. XRD spectra of xRu/TiO_2 samples and TiO_2 references.

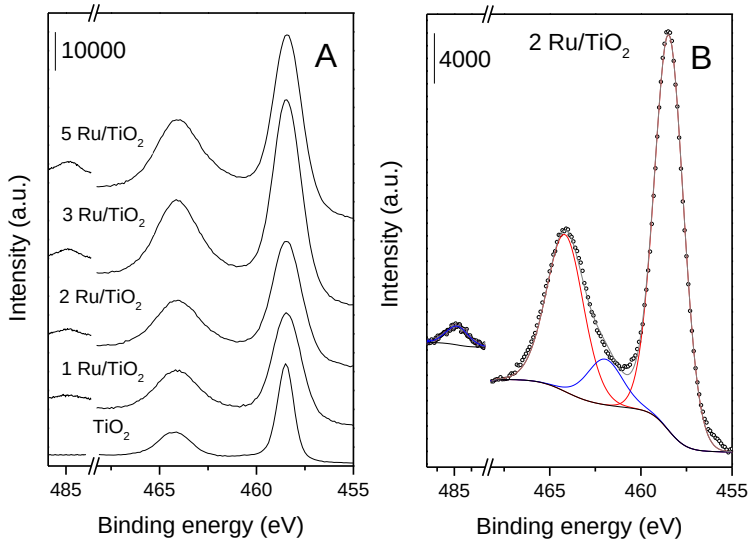

Figure 2. (A) Ti 2p and Ru 3p XPS spectra for the xRu/TiO_2 samples. (B) Representative example of the fitting procedure for the Ti 2p (Red) and Ru 3p (Blue) contributions. (C) C1s and Ru 3d XPS spectra for the xRu/TiO_2 samples. (D) Representative example of the fitting procedure for the C1s (Red) and Ru 3d (Blue) contributions.

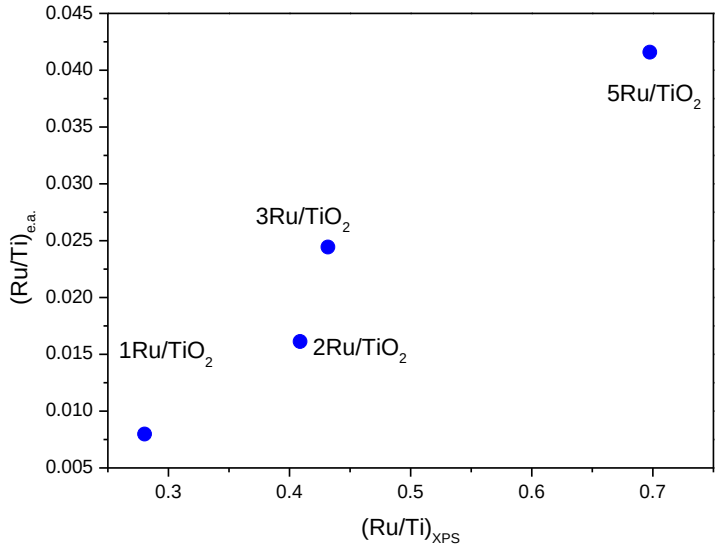

Figure 3. Bulk (Ru/Ti $_{e.a}$) and Superficial (Ru/Ti $_{XPS}$) ratio of the xRu/TiO_2 samples.

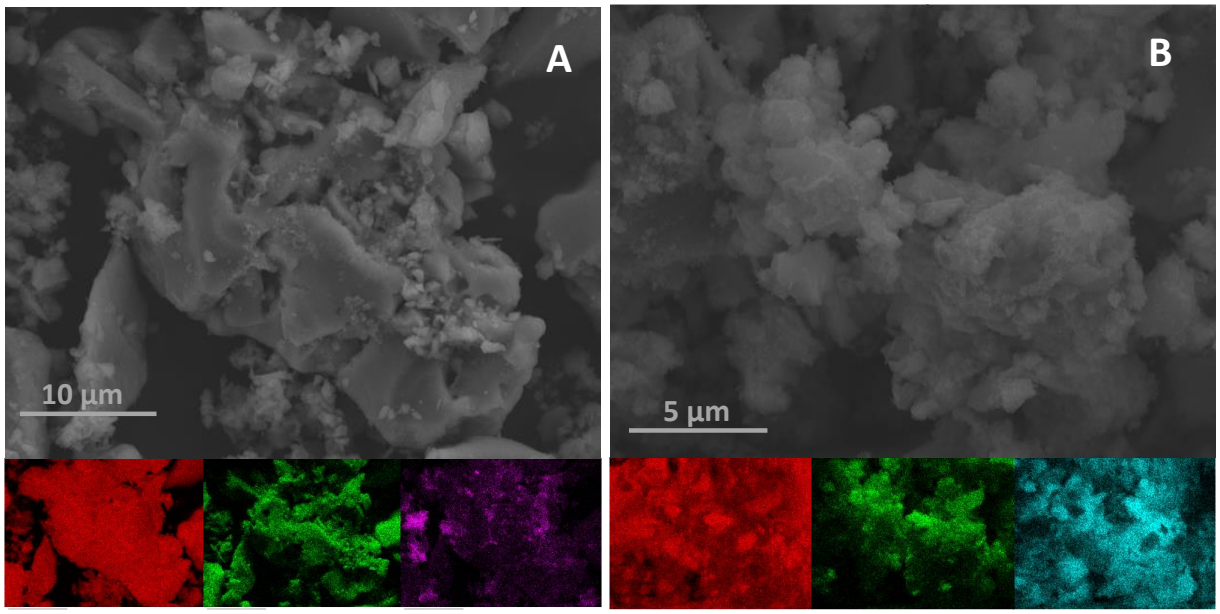

Figure 4. SEM images of 3Ru/TiO_2 (A), and 5Ru/TiO_2 (C). EDX mapping of Ti (red), O (green) and Ru (violet or blue).

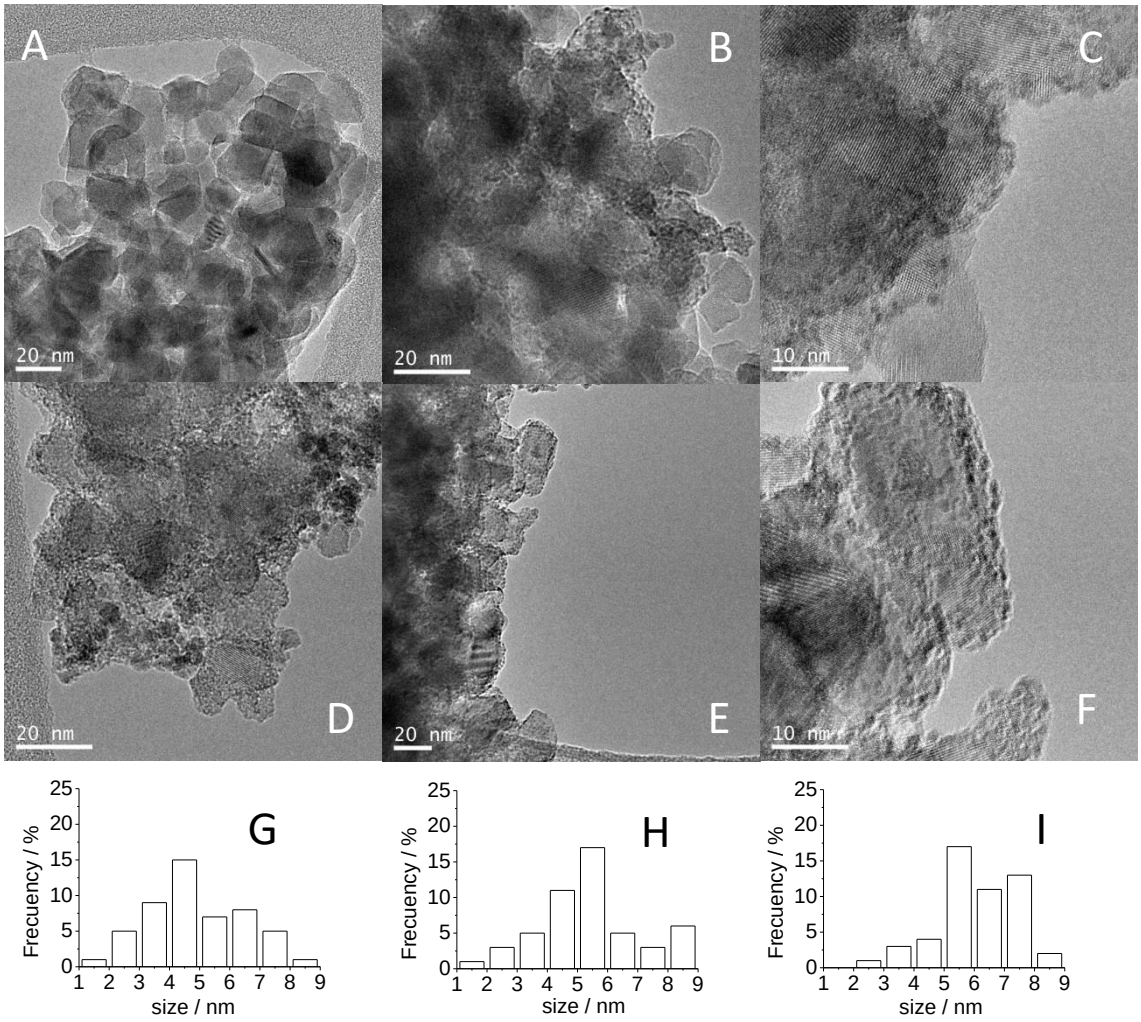

Figure 5. TEM images for the (A-B) 2Ru/TiO_2, (C-D) 3Ru/TiO_2 and (E-F) 5Ru/TiO_2. Ru particle size distributions for (G) 2Ru/TiO_2, (H) 3Ru/TiO_2 and (I) 5Ru/TiO_2.

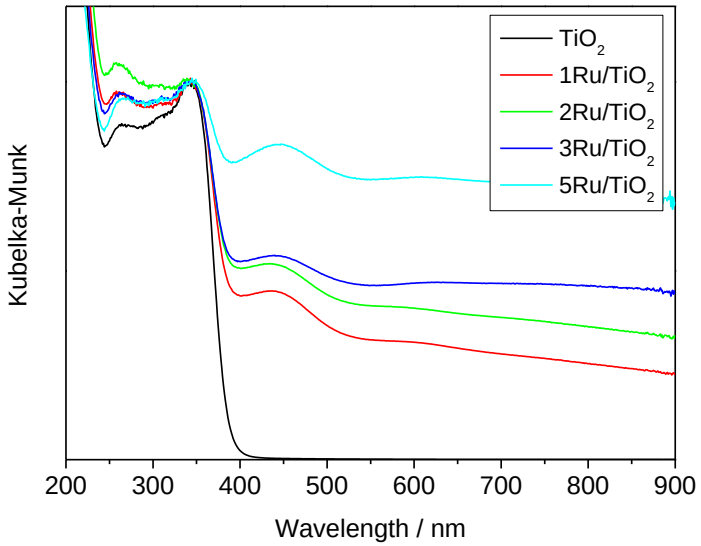

Figure 6. UV-vis spectra of xRu/TiO_2 samples and TiO_2 reference.

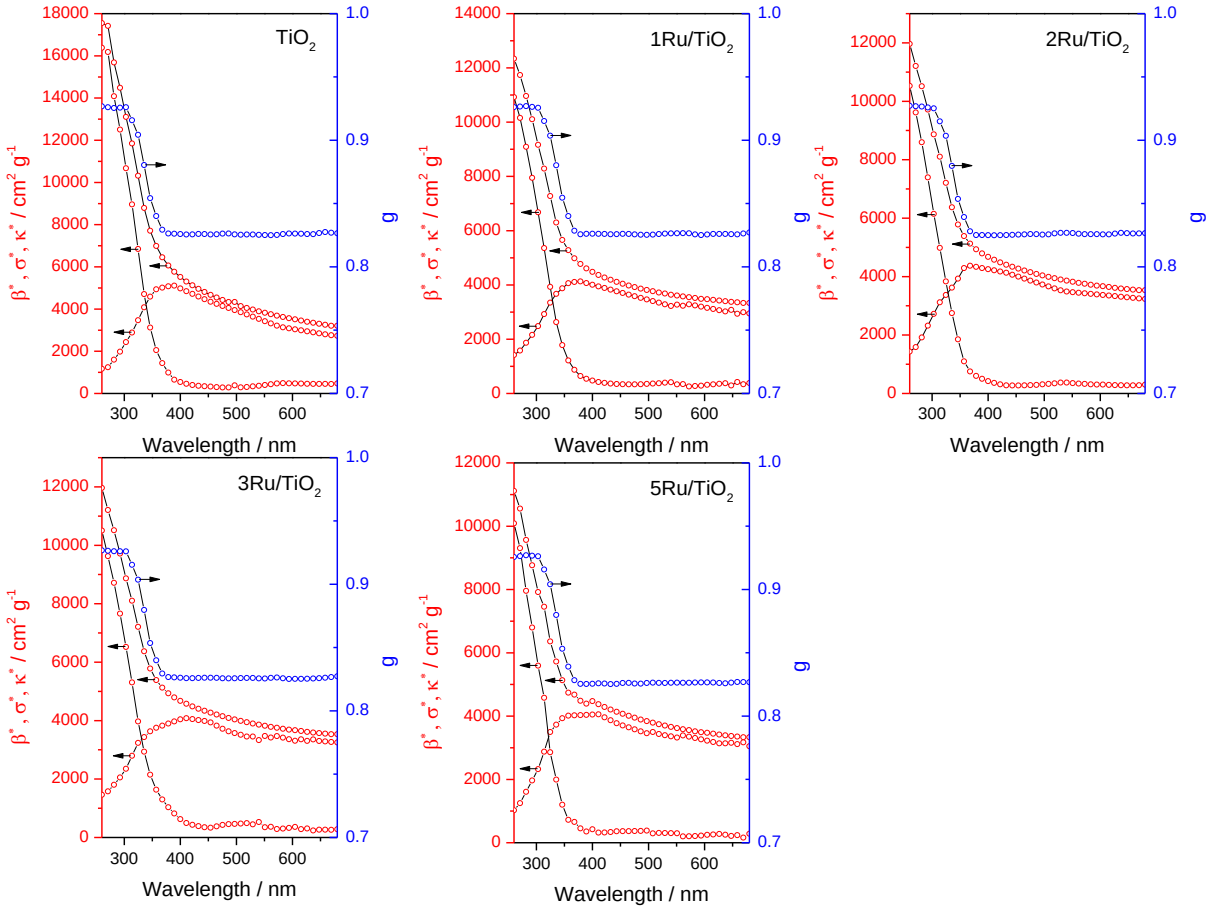

Figure 7. Optical properties of xRu/TiO_2 samples and TiO_2 reference.

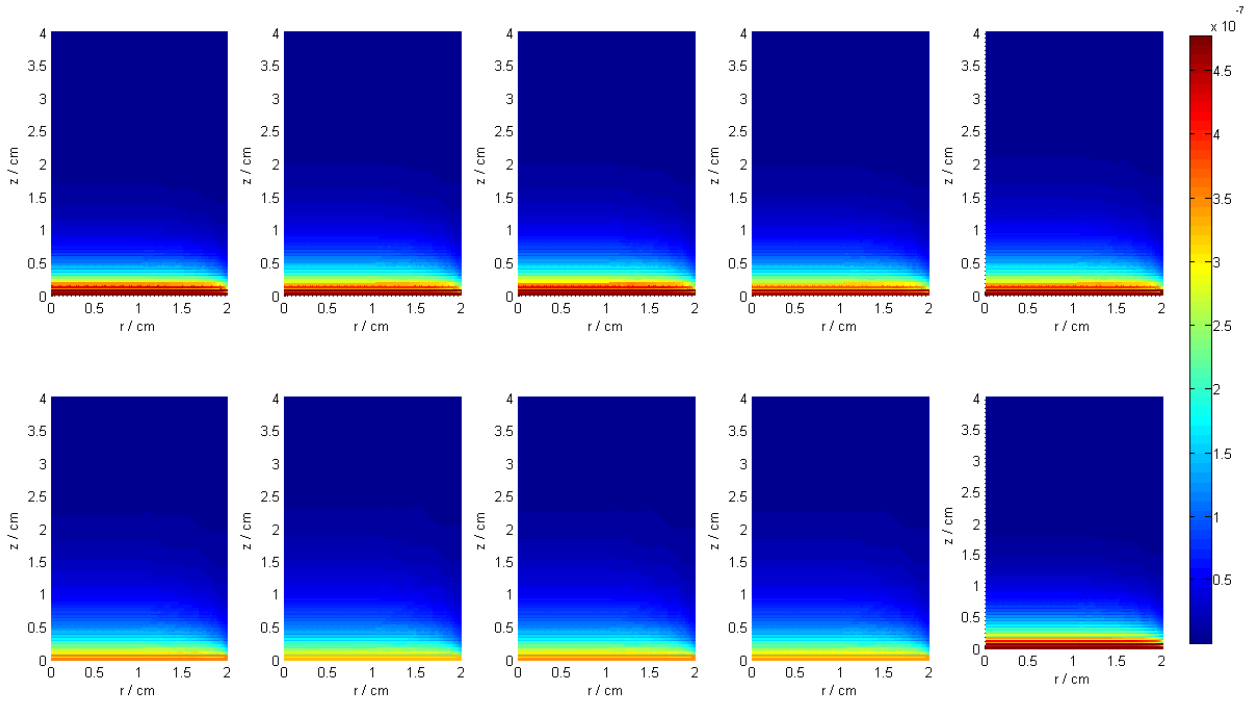

Figure 8. Local volumetric rate of photon absorption (Einstein cm^{-3} s^{-1}). From A to E: TiO_2, $1Ru/TiO_2$, $2Ru/TiO_2$, $3Ru/TiO_2$, $5Ru/TiO_2$ under UV irradiation. From F to J: TiO_2, $1Ru/TiO_2$, $2Ru/TiO_2$, $3Ru/TiO_2$, $5Ru/TiO_2$ under Visible irradiation.

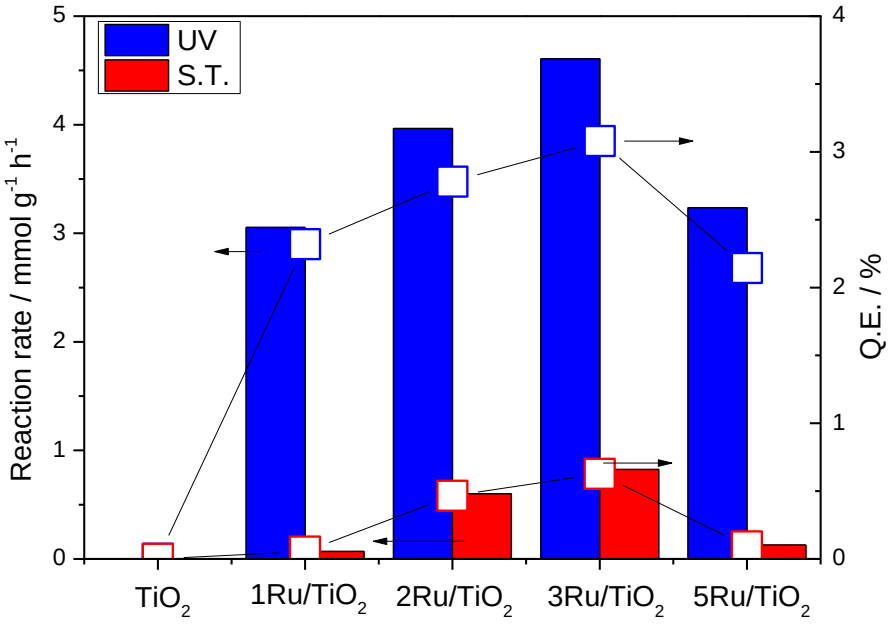

Figure 9. Reaction rate and quantum efficiency obtained under UV and visible illumination for Ru/TiO_2 samples.

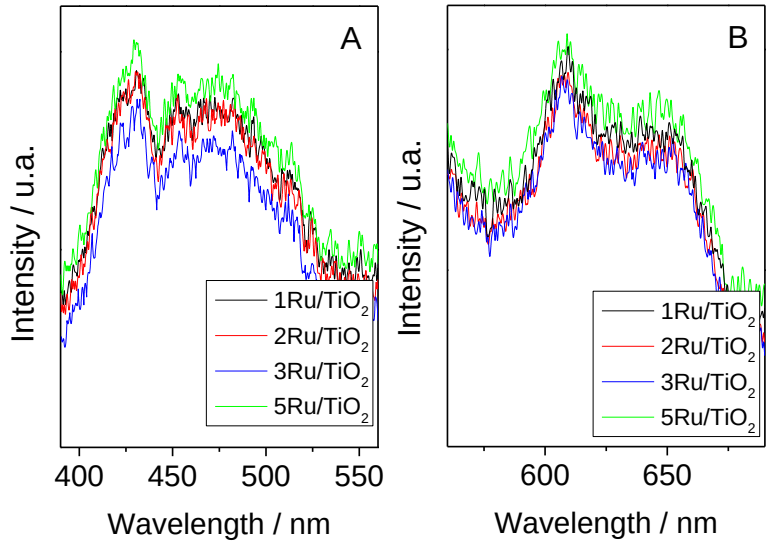

Figure 10. Photoluminescence spectra of samples under UV (A, 320 nm) and Visible (B, 450 nm) excitation.

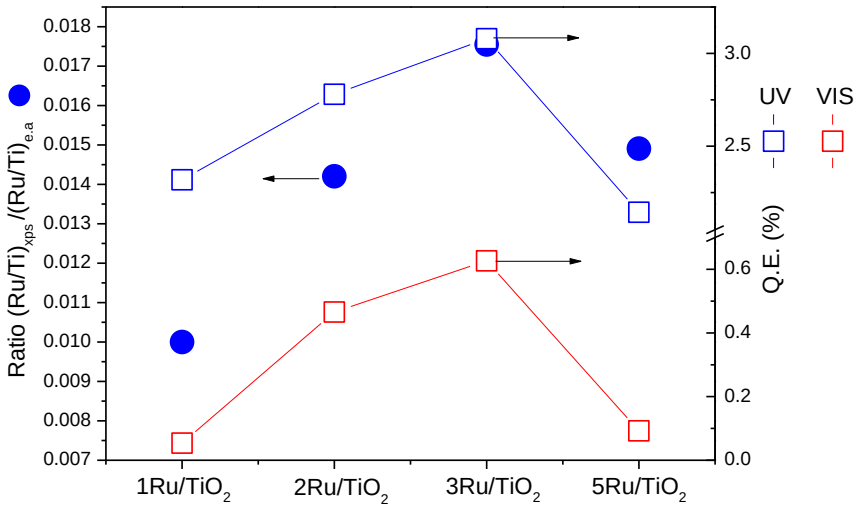

Figure 11. Relationship between the surface (Ru/Ti_{XPS}) and bulk ($Ru/Ti_{e.a}$) Ru/Ti ratios and Quantum Efficiency.

Supplementary Material

Enhancing photocatalytic performance of TiO_2 in H_2 evolution *via* Ru co-catalyst deposition

Weiyi Ouyang,[a] Mario J. Muñoz-Batista,[a] Anna Kubacka,[b] Rafael Luque,[a,c] and Marcos Fernández-García [*b]*

[a]*Departamento de Química Orgánica, Universidad de Córdoba, Edif. Marie Curie, Ctra Nnal IV-A, Km 396, E14014, Córdoba (Spain)*

[b]*Instituto de Catálisis y Petroleoquímica CSIC, Marie Curie 2, 28049 Madrid, Spain.*

[c]*Peoples Friendship University of Russia (RUDN University), 6 Miklukho-Maklaya Str., Moscow 117198, Russia*

Email: M.J. M-B (jmunoz385x@gmail.com), M. F-G (mfg@icp.csic.es)

Abstract

A series of ruthenium catalysts supported into pure anatase oxide were tested in the photo-production of hydrogen from methanol:water mixtures under UV and visible illumination conditions. Catalysts containing 1, 2, 3 and 5 wt.% of ruthenium were subjected to a characterization study with the help of X-ray diffraction, Raman, X-ray photoelectron spectroscopy, photoluminescence, morphology as well as scanning and transmission electron microscopy. Through the measurement of the optical properties of the suspension of the catalysts and the hydrogen photo-production reaction rate we calculate the true quantum efficiency. Optimum activity is presented by the catalyst with a 3 wt.% of Ru component, which shows quantum efficiency values of ca. 3.0 and 0.6 % under, respectively, UV and visible light illumination. Careful examination of the physico-chemical properties of the solid allows to establish a correlation between the ruthenium surface exposed and the quantum efficiency. The implications of such result to justify chemical activity of the ruthenium supported samples are discussed both for UV and visible illumination conditions.

1.- Nomenclature used in the main manuscript

e^a: local volumetric rate of photon absorption (Einstein cm^{-3} s^{-1})
x: x coordinate (cm)
y: y coordinate (cm)
z: z coordinate (cm)
I: specific radiation intensity (Einstein cm^{-2} s^{-1} sr^{-1})
V: Volume (cm^3)

g: asymmetry factor of the Henyey–Greentein's phase function (dimensionless)
p: phase function (dimensionless)
r: radial coordinate (cm)

Greek Letters

β^*: specific extinction coefficient (cm^2 g^{-1})
κ^*: specific absorption coefficient (cm^2 g^{-1})
σ^*: specific scattering coefficient (cm^2 g^{-1})
μ: direction cosine (dimensionless)
Ω: Solid angle (sr)
$\underline{\Omega}$: unit vector in the direction of radiation propagation
β: volumetric extinction coefficient (cm^{-1})
η: direction cosine (dimensionless)
κ: volumetric absorption coefficient (cm^{-1})
λ: wavelength (nm)
σ: volumetric scattering coefficient (cm^{-1})
ω: optical albedo (dimensionless)

Subscripts

λ: denotes wavelength dependence

Special Symbols

$\underline{*}$**:** denotes vector
$\langle * \rangle$: average value over a defined space

2.- Reactor set-up

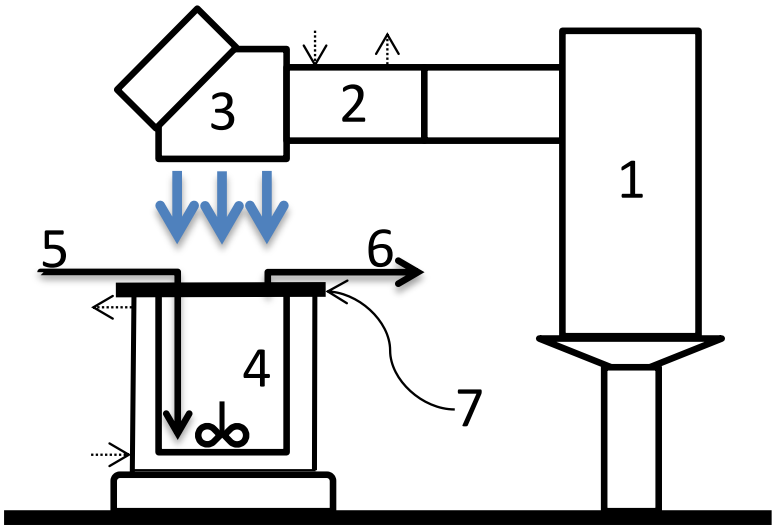

Figure S1. Experimental photoreactor setup. (1) Hg-Xe lamp, (2) Water filter, (3) dichroic filter (280-400; 420-680 nm), (4) Methanol-Water/catalyst suspension, (5) Argon carrier inlet, (6) Argon carrier and gas products outlet, and (7) neutral filter. Dotted arrows indicate inlet and outlet cooling water.

3. Volumetric rate of photon absorption

3.1.Optical properties of the suspension. Solution of RTE for the spectrophotometer cell (one dimensional-one directional model)

The optical properties were obtained by solving the RTE (which consider radiation absorption and scattering effect by the catalyst, Equation 2 of the main manuscript) using the discrete ordinate method (MOD) in a rectangular spectrophotometer cell (0.2 mm optical path) in combination with a nonlinear, multiparameter regression procedure (lsqnonlin (Matlab), Algorithm: Trust-Region-Reflective Optimization). Before that, the extinction coefficients (β^*) were obtained in the spectrophotometer cell by applying a standard linear regression to the plots of β_λ versus catalyst concentration C in a broad range (0.1-5 x 10^{-3} g L^{-1}). Besides, considering that the cell can be represented as an infinite plane parallel medium with azimuthal symmetry, a one-dimensional, one-directional radiation transport model can be used to solve the RTE.

Figure S2A shows a schematic representation of the RTE solution scheme where the net light intensity is presented by one angular-related variable ($\mu = \cos(\theta)$) at each point of the cell one-dimensional (x variable) representation. The fitting procedure renders the values of ω_λ (the so-called albedo defined in equation S1) and g_λ (equation S3, which defines the Henyey–Greentein's scattering phase function: $p(\underline{\Omega}' \rightarrow \underline{\Omega}) =$

$\frac{1-g_\lambda^2}{\left(1+g_\lambda^2-2g_\lambda u_0\right)^{3/2}}$) parameters that minimize the differences between model predictions and experimental data of diffuse transmittance and reflectance measurements at the spectrophotometric cell for a set of catalyst concentrations, C, and in the wavelength range of the light source (1). Then, the volumetric scattering and absorption coefficients can be obtained using Equation S1 and S2 (All optical properties presented in the main text).

$$\sigma_\lambda = \beta_\lambda * \omega_\lambda \quad \text{S1}$$

$$\kappa_\lambda = \beta_\lambda - \sigma_\lambda \quad \text{S2}$$

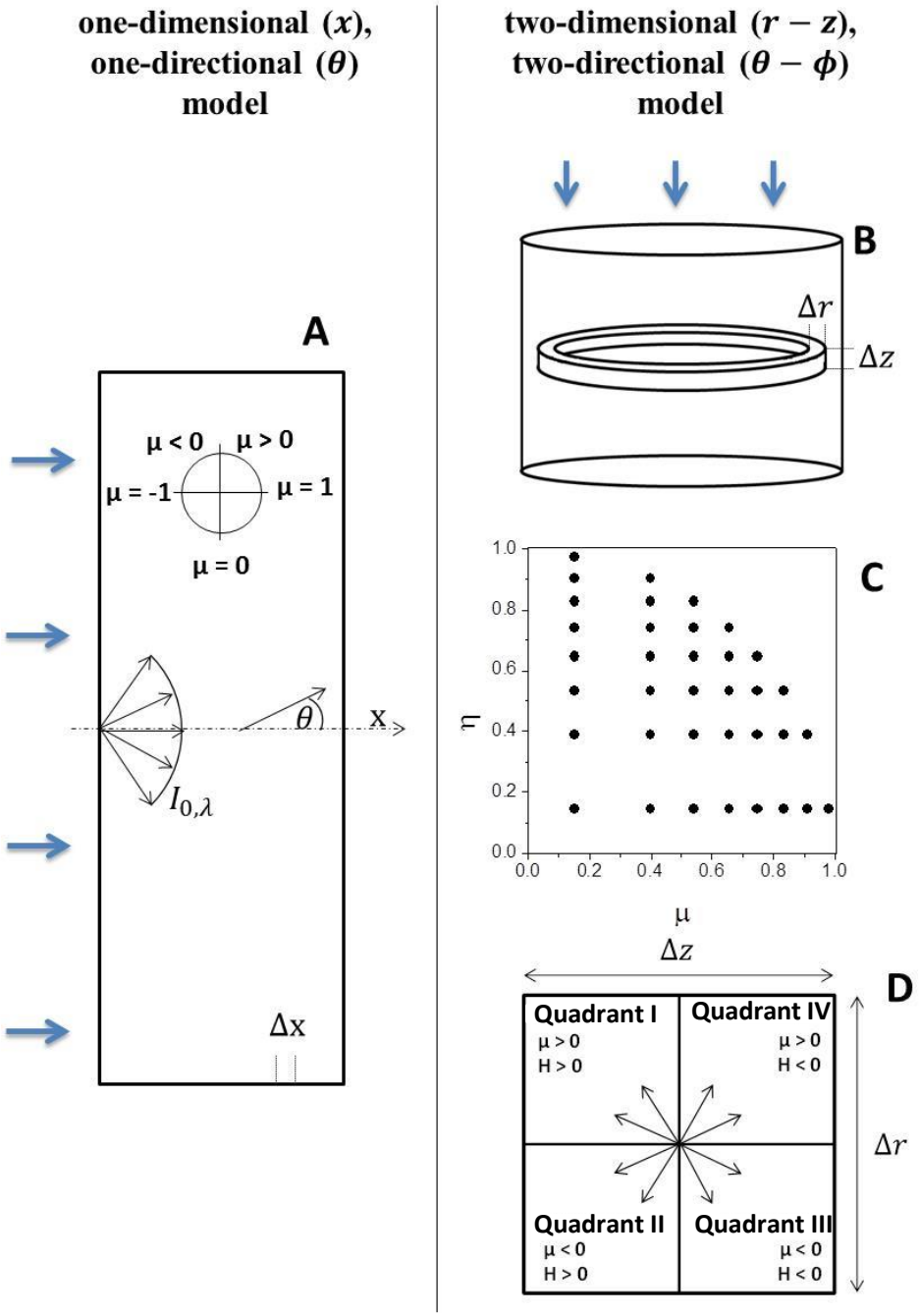

Figure S2. Schematic representation for the one-dimensional, one-directional radiation Model used for the spectrophotometer cell (A) and the two-dimensional, two-directional radiation Model used for the liquid phase photoreactor (B-D). (B) Representation of the r and z spatial mesh discretization of the photoreactor, (C) Directional mesh for the Quadrant I and (D) representation of quadrants of directions as a function of the direction cosines (μ, η) respect to r and z axis in a cross section of the spatial cell.

3.2. Optical properties of the suspension. Solution of RTE for the photoreactor setup (two dimensional-two directional model)

Once the optical properties of the catalyst(s) have been obtained, the evaluation of the radiation field inside the photoreactor presented in Figure S1 can be carried out. The MOD tool was used to transform the integro-differential equation 2 (main text) into a system of algebraic equations that can be solved numerically. Our reactor configuration requires the use of a cylindrical two-dimensional ($r-z$ variables), two-directional ($\theta-\phi$ variables) model of the photoreactor radiation field (Figure S2B-C). The net radiation intensity at each $r-z$ point of the reactor is now represented using a discretized spatial mesh having two angular-related coordinates $\mu = \cos(\theta)$; $\eta = \cos(\phi)$. Fig. S2C displays μ; η unitary, basal projection(s) in a quadrant of the space around a $r-z$ point calculated using the so-called S_{16} method (2). The computation of the intensity at each point of the reactor require to divide the space in 4 quadrants as depicted in Figure 2D and the measurement of the incident light intensity at the frontier (liquid surface) using actinometry (2). According to the Duderstadt and Martin recommendation (3), and following the numerical procedure scheme detailed by previous authors (2), the finite difference (MOD) was derived directly from the radiation balance for each mesh cell (Figure S2D). The solution of Equation 2 of the main text provides the light intensity $I_{\lambda,\underline{\Omega}}(\underline{x}; r-z)$ at each point of the reactor.

Finally, once the intensities were obtained, the local volumetric rate of photon absorption (e^a) was calculated at each $r-z$ point of the reactor according to:

$$e^a = \int_\lambda \kappa_\lambda \cdot \int_{\Omega=4\pi} I_{\lambda,\underline{\Omega}}(\underline{x}) d\Omega \, d\lambda \qquad \text{S4}$$

4.- Raman analysis of titania support

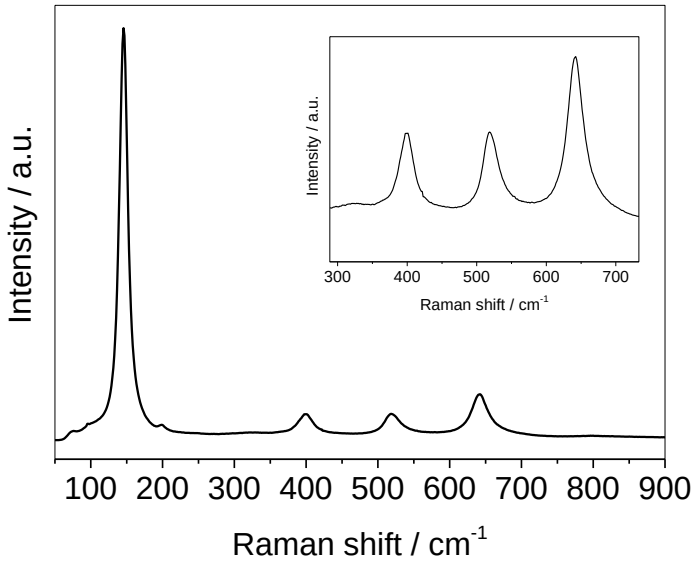

Figure S3. Raman spectrum of TiO_2 pure reference.

5.- Quantum Efficiency and Photonic Efficiency calculations

Q.E. (**Quantum Efficiency**) and P.E (**Photonic Efficiency, also called Apparent Quantum Efficiency**) definitions are:

$$Q.E.(\%) = 100 \times \frac{n \times r\ (\mathrm{mol\ m^{-3}s^{-1}})}{e^a\ (\mathrm{Einstein\ m^{-3}s^{-1}})} \qquad \text{S5 (Equation 1 in the main text)}$$

$$P.E.(\%) = 100 \times \frac{n \times r\ (\mathrm{mol\ m^{-2}s^{-1}}) \times V\ (\mathrm{m^3})}{q\ (\mathrm{Einstein\ m^{-3}s^{-1}}) \times A\ (\mathrm{m^2})} \qquad \text{S6}$$

Where, r is the reaction rate, e^a is the local volumetric rate of photon absorption, V is the reactor volume, and q represents the incident radiation flux averaged in the illuminated reactor surface (A). q value experimentally measured using a radiometer (Delta OHM) at the sample average position were 1.8×10^{-7} and 2.9×10^{-7} Einstein cm^{-2} s^{-1} for, respectively, UV and ST illumination conditions. n takes the value 1 or 2 depending on the mechanism (See the discussion in the main text for details).

Table S1. Quantum Efficiency and Photonic Efficiency under UV and Sunlight-type (S.T.) illumination conditions.[a]

Sample	UV Q.E. (%) n=2[b]/ n=1[c]	UV P.E. (%) n=2[b]/ n=1[c]	S.T. Q.E. (%) n=2[b]/ n=1[c]	ST P.E. (%) n=2[b]/ n=1[c]
1Ru/TiO_2	2.3/1.2	1.9/1.0	0.05/0.0_3	0.04/0.0_2
2Ru/TiO_2	2.8/1.4	2.4/1.2	0.5/0.3	0.4/0.2
3Ru/TiO_2	3.1/1.6	2.8/1.4	0.6/0.3	0.5/0.3
5Ru/TiO_2	2.1/1.1	2.0/1.0	0.1/0.0_5	0.08/0.0_4

[a] Standard error: Q.E. (%) <15%; P.E. (%)<12%. [a] Gaussian-type standard errors were estimated using the equations reported in [4]. [b]Quantum Efficiency calculated using n = 2 (see details in the main text), [c]Quantum Efficiency calculated using n = 1(see details in the main text).

6. Mechanism

Table S2. H_2 photoprodution mechanism scheme.

Step	Number
$Catalyts + hv \rightarrow e^- + h^+$	1
$e^- + h^+ \rightarrow calor$	2
$H_2O_{ads} + h^+ \rightarrow OH^{\bullet}_{ads} + H^+_{ads}$	3
$CH_3OH_{ads} + OH^{\bullet}_{ads}(h^+) \rightarrow CH_3O^{\bullet} + H_2O_{ads}(H^+_{ads})$	4
$CH_3OH_{ads} + OH^-_{ads} \rightarrow CH_3O^-_{ads} + H_2O_{ads}$	5
$CH_3O^{\bullet} + CH_3O^-_{ads} + H^+ \rightarrow 2\,CH_2O_{ads} + H^+ + e^-$	6
$CH_3O^{\bullet}_{ads} + OH^{\bullet}_{ads}(h^+) \rightarrow CH_2O_{ads} + H_2O_{ads}(H^+_{ads})$	7
$CH_2O_{ads} + OH^{\bullet}_{ads}(h^+) \rightarrow HCO^{\bullet}_{ads} + H_2O_{ads}(H^+_{ads})$	8
$HCO^{\bullet}_{ads} + OH^{\bullet}_{ads} \rightarrow HCOOH_{ads}$	9
$HCOOH_{ads} + OH^{\bullet}_{ads}(h^+) \rightarrow {}^{\bullet}COOH_{ads} + H_2O_{ads}(H^+_{ads})$	10
${}^{\bullet}COOH_{ads} + OH^{\bullet}_{ads}(h^+) \rightarrow CO_{2_{ads}} + H_2O_{ads}(H^+_{ads})$	11
$2H^+_{ads} + 2e^- \rightarrow H_2$	12

References

1 M.I. Cabrera, O.M. Alfano, A.E. Cassano, J. Phys. Chem. 100 (1996) 20043–20050.

2 (a) R.L Romero, O.M. Alfano, A.E. Cassano, Ind. Eng. Chem.. Res. 36 (1997) 3094-3109; (b) Marugán, R. van Grieken, A.E. Cassano, O.M. Alfano, Appl. Catal. B 85 (2008) 48-60.

3 J.J. Duderstadt, W.R. Martin, Transport Theory, Wiley, New York, 1979.

4 M.J. Muñoz-Batista, A. Kubacka, A.B. Hungría, M. Fernández-García, Heterogeneous photocatalysis: Light-matter interaction and chemical effects in quantum efficiency calculations, J. Catal. 330 (2015) 154–166.